Hindawi
Advances in High Energy Physics
Volume 2020, Article ID 1787183, 14 pages
https://doi.org/10.1155/2020/1787183

Research Article

Kinetic Freeze-Out Temperature and Transverse Flow Velocity in Au-Au Collisions at RHIC-BES Energies

Muhammad Waqas and Bao-Chun Li

Institute of Theoretical Physics & Department of Physics & State Key Laboratory of Quantum Optics and Quantum Optics Devices, Shanxi University, Taiyuan, Shanxi 030006, China

Correspondence should be addressed to Bao-Chun Li; libc2010@163.com

Received 25 September 2019; Revised 21 November 2019; Accepted 13 December 2019; Published 8 January 2020

Guest Editor: Raghunath Sahoo

By using the method of data-driven reanalysis, the midrapidity transverse momentum (p_T) spectra of charged hadrons (π^+, K^+, and p) produced in central and peripheral gold-gold (Au-Au) collisions from the Beam Energy Scan (BES) program at the Relativistic Heavy Ion Collider (RHIC) are fitted by using the blast-wave model with the Boltzmann-Gibbs statistics. The model results are in agreement with the experimental data measured by the STAR Collaboration at the RHIC-BES energies. We observe that the kinetic freeze-out temperature (T_0), transverse flow velocity (β_T), mean transverse momentum ($\langle p_T \rangle$), and initial temperature (T_i) increase with collision energy as well as with event centrality.

1. Introduction

One of the most fundamental questions in high energy and nuclear physics is to determine the phase structure of the strongly interacting quantum chromodynamics (QCD) matter [1–3]. The yield ratios, transverse momentum (p_T) spectra, and other data for various identified particles produced in proton-proton (pp), proton-nucleus (pA), and nucleus-nucleus (AA) collisions at high energies are important observable quantities for determining the phase structure. The experimental facilities such as the Relativistic Heavy Ion Collider (RHIC) and the Large Hadron Collider (LHC) provide excellent tools to study the properties of Quark-Gluon Plasma (QGP) [4–6], which are expected to create collision events with high multiplicities.

The phase diagram of the QCD matter is usually expressed in terms of the chemical freeze-out temperature (T_{ch}) and the baryon chemical potential (μ_B) [7, 8]. Besides, other quantities such as the kinetic freeze-out temperature (T_{kin} or T_0) and transverse flow velocity (β_T) are useful to understand the phase diagram [9]. To search for the possible critical energy in the phase transition from hadronic matter to QGP in high-energy collisions, the STAR Collaboration has been performing the Beam Energy Scan (BES) program [10–13] at the RHIC. Besides, other experiments at similar or lower energies at other accelerators are scheduled [14, 15].

Generally, the processes of high-energy collisions result possibly in three main stages [16–18]:

(i) The initial stage: at this stage, the collisions are in the beginning. The temperature at this stage is called the initial temperature which is one of the main factors to affect the particle spectra, which is less studied in the community comparatively. After the initial state, the "fireball" leads to a decrease in the temperature and finally to the hadronization

(ii) The chemical freeze-out stage: at this stage, the inner collisions among various particles are elastic and the yield ratios of differential types of particles remain invariant. The chemical freeze-out temperature T_{ch} can be obtained from the particle ratios, which is much studied in the community comparatively

(iii) The kinetic freeze-out stage: at this stage, the scattering processes stop, the hadrons decouple from the rest of the system, and the hadron's energy/momentum

spectra freeze in time. The temperature at this stage is known as the kinetic freeze-out temperature T_0 which can be obtained from the p_T spectra

When one studies T_0 from the p_T spectra, the effect of β_T should be eliminated. If the effect of β_T is not eliminated in the temperature, this temperature is called the effective temperature (T_{eff} or T). At the stage of kinetic freeze-out, T_0 and β_T are two important parameters which describe the thermal motion of the produced particles and the collective expansion of the emission source, respectively. The spectra in a low-p_T region ($p_T = 2 - 3$ GeV/c) which is mainly contributed by the soft excitation process essentially separate the contribution of the thermal motion and the collective expansion, if one only extracts T_0 and β_T. The spectra in a high-p_T region are contributed by the hard scattering process which is not needed in extracting T_0 and β_T.

We are very interested in the extraction of T_0 and β_T in collisions at the RHIC-BES energies which are very suitable to study the spectra in a low-p_T region, where the spectra in a high-p_T region are not produced due to not too high energies. In this work, the double-differential p_T spectra of charged particle dependences on collision energy and event centrality in gold-gold (Au-Au) collisions are analyzed with the blast-wave model with the Boltzmann-Gibbs statistics by means of data-driven analysis. The model results are compared with the data measured by the STAR Collaboration at the RHIC-BES energies [19, 20].

The remainder of this work consists of The Method and Formalism, Results and Discussion, and Conclusions. We shall describe the remanent parts orderly.

2. The Method and Formalism

Various methods can be used for the extraction of T_0 and β_T, e.g., the blast-wave model with the Boltzmann-Gibbs statistics [21–23], the blast-wave model with the Tsallis statistics [24–26], an alternative method by using the Boltzmann-Gibbs statistics [22, 27–33], and the alternative method by using the Tsallis distribution [33–39]. In this work, we choose the blast-wave model with the Boltzmann-Gibbs statistics due to its similarity with the ideal gas model in thermodynamics and few parameters. However, these methods only describe the spectra in the low-p_T region. For the spectra in the high-p_T region if available, the Hagedorn function which is known as the inverse power law [40, 41] can be used. We shall discuss these issues in detail as follows.

In general, there are two main processes responsible for the contribution of p_T spectra. They are (i) the soft excitation process which contributes the soft component in the low-p_T region and (ii) the hard scattering process which contributes the hard component in the whole p_T region if one uses the general superposition function or in the high-p_T region if one uses the usual step function.

For the soft component, according to Refs. [21–23], the probability density function of the p_T spectra in the blast-wave model with the Boltzmann-Gibbs statistics results in

$$f_1(p_T) = \frac{1}{N}\frac{dN}{dp_T} = C_{p_T m_T}\int_0^R r dr \times I_0\left[\frac{p_T \sinh(\rho)}{T_0}\right] K_1\left[\frac{m_T \cosh(\rho)}{T_0}\right], \quad (1)$$

where N is the number of particles, C is the normalization constant, $m_T = \sqrt{p_T^2 + m_0^2}$ is the transverse mass, m_0 is the rest mass of the considered particle, r and R are the radial position and the maximum radial position, respectively, I_0 and K_1 are the modified Bessel functions of the first and second kinds, respectively, $\rho = \tanh^{-1}[\beta(r)]$ is the boost angle, $\beta(r) = \beta_S(r/R)^{n_0}$ is a self-similar flow profile, β_S is the flow velocity on the surface, and $n_0 = 2$ is used in the original form [21]. Particularly, $\beta_T = (2/R^2)\int_0^R r\beta(r)dr = 2\beta_S/(n_0+2) = 0.5\beta_S$. The parameter n_0 is used in different works, e.g., $n_0 = 1$ or noninteger in Refs. [22, 24, 42], which corresponds to the centrality from the center to the periphery.

Equation (1) and similar or related functions are not enough to describe the whole p_T spectra. In particular, the maximum p_T reaches up to 100 GeV/c in collisions at the LHC [43]. Then, one needs other functions such as the Tsallis–Lévy- [44, 45] or Tsallis–Pareto-type function [44, 46] and the Hagedorn function [40, 41] or inverse power law [47–49] to the spectra in high- and very high-p_T regions. In this work, the hard component is simply represented by the inverse power law. That is,

$$f_2(p_T) = \frac{1}{N}\frac{dN}{dp_T} = Ap_T\left(1 + \frac{p_T}{p_0}\right)^{-n}, \quad (2)$$

where p_0 and n are free parameters and A is the normalization constant which is related to the free parameters.

However, the structure of p_T spectra is very complex. In fact, several regions have been observed and analyzed in Ref. [50]. These regions include the first one with $p_T < 4 - 6$ GeV/c, the second one with $4 - 6$ GeV/$c < p_T < 17 - 20$ GeV/c, and the third one with $p_T > 17 - 20$ GeV/c. Different regions may correspond to different mechanisms. The first p_T region in our discussion is regarded as the region of the soft excitation process, while the second and third p_T regions are regarded as the regions of the hard and the very hard excitation process, respectively. In particular, a special region with $p_T < 0.2 - 0.3$ GeV/c is considered due to the resonant production in some cases, and it is regarded as the region of the very soft excitation process.

Generally, the whole p_T region discussed above can be uniformly superposed by two methods: (i) the general superposition in which the contribution regions of different components overlap each other and (ii) the Hagedorn model (the usual step function) [40] in which there is no overlapping of different regions of different components.

Considering $f_1(p_T)$, $f_2(p_T)$, $f_{VS}(p_T)$, and $f_{VH}(p_T)$ which denote the probability density functions by the soft, hard, very soft, and very hard components, respectively, where

$f_{\rm VS}(p_{\rm T})$ and $f_{\rm VH}(p_{\rm T})$ are assumed to be in the form of $f_1(p_{\rm T})$ and $f_2(p_{\rm T})$, respectively, the unified superposition according to the first method is

$$f_0(p_{\rm T}) = \frac{1}{N}\frac{dN}{dp_{\rm T}} = k_{\rm VS} f_{\rm VS}(p_{\rm T}) + k f_1(p_{\rm T}) + (1 - k - k_{\rm VS} - k_{\rm VH}) f_2(p_{\rm T}) + k_{\rm VH} f_{\rm VH}(p_{\rm T}), \quad (3)$$

where $k_{\rm VS}$ is the contribution fraction of the very soft component, while k and $k_{\rm VH}$ denote the contributions of the soft and very hard components, respectively.

The step function can be used to structure the superposition according to the Hagedorn model [40]; i.e.,

$$f_0(p_{\rm T}) = \frac{1}{N}\frac{dN}{dp_{\rm T}} = A_{\rm VS}\theta(p_{\rm VS} - p_{\rm T}) f_{\rm VS}(p_{\rm T}) + A_1\theta(p_{\rm T} - p_{\rm VS})\theta(p_1 - p_{\rm T}) f_1(p_{\rm T}) + A_2\theta(p_{\rm T} - p_1)\theta(p_{\rm VH} - p_{\rm T}) f_2(p_{\rm T}) + A_{\rm VH}\theta(p_{\rm T} - p_{\rm VH}) f_{\rm VH}(p_{\rm T}), \quad (4)$$

where $A_{\rm VS}$, A_1, A_2, and $A_{\rm VH}$ are the constants which make the interfacing components link to each other perfectly.

Particularly, if the contributions of the very soft and very hard components can be neglected, Equations (3) and (4) are, respectively, simplified to be

$$f_0(p_{\rm T}) = \frac{1}{N}\frac{dN}{dp_{\rm T}} = k f_1(p_{\rm T}) + (1 - k) f_2(p_{\rm T}), \quad (5)$$

$$f_0(p_{\rm T}) = \frac{1}{N}\frac{dN}{dp_{\rm T}} = A_1\theta(p_1 - p_{\rm T}) f_1(p_{\rm T}) + A_2\theta(p_{\rm T} - p_1) f_2(p_{\rm T}). \quad (6)$$

Further, if the contribution of the hard component at the RHIC-BES energies can be neglected, Equations (5) and (6) are simplified to be the same form:

$$f_0(p_{\rm T}) = \frac{1}{N}\frac{dN}{dp_{\rm T}} = f_1(p_{\rm T}). \quad (7)$$

This work deals with Au-Au collisions at the RHIC-BES energies, for which Equation (7), i.e., Equation (1), is suitable. In the following section, we shall use Equation (1) to fit the experimental data measured by the STAR Collaboration at the RHIC-BES energies [19, 20].

In particular, the mean $p_{\rm T}(\langle p_{\rm T}\rangle)$ and the root-mean-square $p_{\rm T}(\sqrt{\langle p_{\rm T}^2\rangle})$ can be expressed, respectively, as

$$\langle p_{\rm T}\rangle = \int_0^{p_{\rm T\ max}} p_{\rm T} f_0(p_{\rm T}) dp_{\rm T}, \quad (8)$$

$$\sqrt{\langle p_{\rm T}^2\rangle} = \sqrt{\int_0^{p_{\rm T\ max}} p_{\rm T}^2 f_0(p_{\rm T}) dp_{\rm T}}, \quad (9)$$

due to

$$\int_0^{p_{\rm Tmax}} f_0(p_{\rm T}) dp_{\rm T} = 1, \quad (10)$$

where $p_{\rm Tmax}$ denotes the maximum $p_{\rm T}$ considered by us. In this work, we take $p_{\rm Tmax} = 2.5$ GeV/c.

It should be noted that although only Equation (1) is used in the analysis, we would like to continue to have the statement and formalism for other functions or distributions such as the inverse power law and its superposition with thermal distribution and the discussions on the very soft, hard, and very hard components. In fact, due to the existence of other functions or distributions, the mentioned method of data-driven reanalysis can be used in the spectra in wide $p_{\rm T}$ coverage, which is not the case in this work. In addition, it is possible to use simultaneously the (very) soft and (very) hard components in other cases which are more universal.

3. Results and Discussion

Figure 1 presents the event centrality-dependent double-differential $p_{\rm T}$ spectra, $(1/2\pi p_{\rm T})d^2N/dp_{\rm T}dy$, of π^+, K^+, and p produced in the midrapidity interval $|y| < 0.1$ in Au-Au collisions at the center-of-mass energy per nucleon pair $\sqrt{sNN} = 7.7$ GeV at the RHIC-BES, where y denotes the rapidity. The symbols represent the experimental data measured by the STAR Collaboration [19], and the curves are our fitting results by using the blast-wave model with the Boltzmann-Gibbs statistics, Equation (1) [21–23]. The spectra in centrality classes 0–5%, 5–10%, 10–20%, 20–30%, 30–40%, 40–50%, 50–60%, 60–70%, and 70–80% are scaled by 1, 1/2, 1/4, 1/6, 1/8, 1/10, 1/12, 1/14, and 1/16, respectively. In the fit, the least-square method is used to determine the best values of parameters. The related parameters along with χ^2 and degree of freedom (dof) are listed in Table 1, where the centrality classes are listed together. One can see that Equation (1) fits well the data in Au-Au collisions at 7.7 GeV at the RHIC.

Figure 2 is the same as Figure 1, but it shows the $p_{\rm T}$ spectra at $\sqrt{sNN} = 11.5$ GeV. One can see that Equation (1) fits well the data in Au-Au collisions at 11.5 GeV at the RHIC-BES.

Figure 3 is also the same as Figure 1, but it shows the $p_{\rm T}$ spectra at $\sqrt{sNN} = 14.5$ GeV, where the data are cited from Ref. [20]. Once again, Equation (1) fits well the data in Au-Au collisions at 14.5 GeV at the RHIC-BES.

Figures 4–6 are also the same as Figure 1, but they show the $p_{\rm T}$ spectra at $\sqrt{sNN} = 19.6$, 27, and 39 GeV, respectively. Once more, Equation (1) fits well the data in Au-Au collisions at other RHIC-BES energies.

It is noteworthy to point out that Equation (1) for the blast-wave model in the system is assumed to be in local thermodynamic equilibrium, and therefore, a single T_0 and $\beta_{\rm T}$ should be obtained by the weight average of different particle species. To see clearly the trends of weight average parameters, Figures 7(a) and 7(b) show the dependences of weight averages T_0 and $\beta_{\rm T}$ on $\sqrt{sNN}$ for different event centralities.

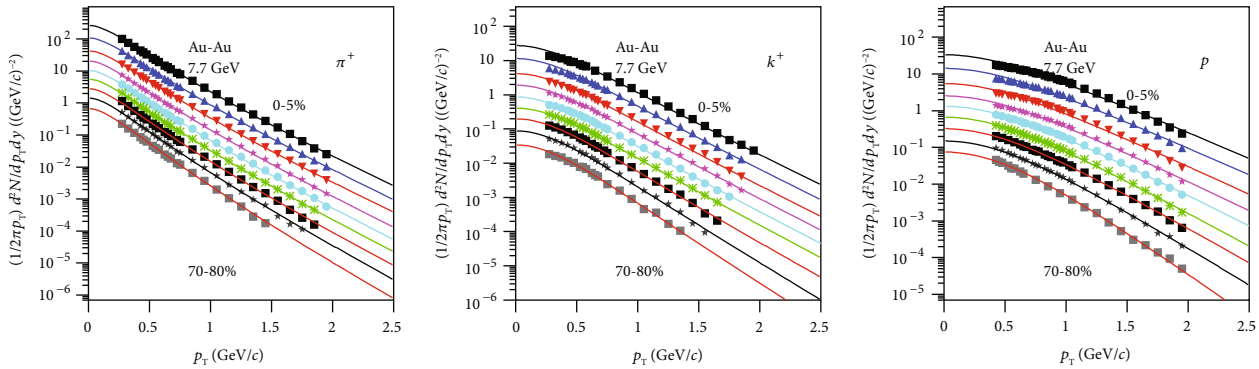

FIGURE 1: Transverse momentum spectra of (a–c) π^+, K^+, and p produced in different centrality bins in Au-Au collisions at $\sqrt{sNN} = 7.7$ GeV. The symbols represent the experimental data measured by the STAR Collaboration in the midrapidity interval $|y| < 0.1$ [19]. The curves are our fitted results by Equation (1).

The symbols represent the parameter values averaged by weighting the yields of different particles which are listed in Table 1. One can see that T_0 and β_T increase with the increase in $\sqrt{sNN}$ from 7.7 to 39 GeV. Meanwhile, T_0 and β_T increase with the increase in the event centrality from the periphery to the center.

In addition, the variation of weight averages T_0 on β_T for different collision energies and event centralities is displayed in Figure 7(c), where the symbols represent the parameter values averaged by weighting the yields of different particles. One can see that T_0 increases with the increase in β_T. At higher energy and in central collisions, one sees larger T_0 and β_T. There is a positive correlation between T_0 and β_T.

The dependences of mean transverse momentum ($\langle p_T \rangle$) and initial temperature (T_i) on $\sqrt{sNN}$ for different event centralities obtained by weighting the yields of different particles are shown in Figures 8(a) and 8(b), respectively, where $T_i = \sqrt{\langle p_T^2 \rangle/2}$ according to the color string percolation model [51–53]. One can see that $\langle p_T \rangle$ and T_i increase with the increase in $\sqrt{sNN}$ from 7.7 to 39 GeV. Meanwhile, $\langle p_T \rangle$ and T_i increase with the increase in event centrality from the periphery to the center.

We notice that $T_i = 0.28 - 0.38$ GeV which is quite high for the considered collision energies. Because we obtain T_i from the spectra of particles with nonzero masses, it is possible to have a high value. If we obtain T_i from the spectra of photons, the value will be small. High T_i renders that the excitation degree of the emission source at the stage of the initial state is high. Meanwhile, one of the key issues is whether the transverse flow should be also considered at the initial stage. Naturally, after considering the transverse flow at the initial stage, T_i will be small. It is regretful that we have no clear idea on the extraction of transverse flow at the initial stage. As an alternative method, if we redefine $T_i = k_0\sqrt{\langle p_T^2 \rangle/2}$ as the initial temperature and $\beta_{Ti} = (1 - k_0)\sqrt{\langle p_T^2 \rangle/2}$ as the initial transverse flow velocity, where $0 < k_0 < 1$ is to be determined, we may obtain a small T_i and a nonzero β_{Ti}.

The reason for the increase in T_0 and β_T with the increase in collision energy is due to the fact that more energies are deposited in collisions at higher energy in the considered RHIC-BES energy range. Meanwhile, the system size at higher energy decreases due to a relativistic constriction effect, which results in a smaller volume and then a larger energy density and larger T_0. Meanwhile, at higher energy, the squeeze is more violent, which results in a rapider expansion and larger β_T.

The reason for the increase in T_0 and β_T with the increase in event centrality is due to the fact that the central collisions contain more nucleons than the peripheral collisions; then, more energies are deposited in central collisions. Meanwhile, a rapider expansion appears due to more violent squeeze in central collisions, compared to peripheral collisions. As a result, both T_0 and β_T in central collisions are larger than those in peripheral collisions.

Because of $\langle p_T \rangle$ and T_i being positive correlation with T_0 and β_T, with increasing collision energy and event centrality, the increasing trend of T_0 and β_T results naturally in the increasing trend of $\langle p_T \rangle$ and T_i. This work shows that the two free parameters T_0 and β_T and the two derived parameters $\langle p_T \rangle$ and T_i appear to be similar law on the dependences of collision energy and event centrality. In particular, $\langle p_T \rangle$ and T_i are model-independent, though we obtain them from model-dependent free parameters T_0 and β_T in this work. In fact, $\langle p_T \rangle$ and T_i can be obtained by the p_T data themselves if the data are across the possible p_T range.

It seems that there are nonmonotonous changes at 11.5 GeV in the excitation functions of β_T, $\langle p_T \rangle$, and T_i in the most central Au-Au collisions. These nonmonotonous changes reflect the minimum or maximum point of equation of state (EoS) of the matter formed in collisions. At a few GeV to about 10 GeV, the matter formed in collisions is baryon-dominant. At above 10 GeV, the matter formed in collisions is meson-dominant. At around 10 GeV, the baryon number density is the largest [54] due to the competition between projectile/target penetrating/stopping and longitudinal contraction.

Table 1: Values of free parameters (T_0 and β_T), normalization constant (N_0), χ^2, and dof corresponding to the curves in Figures 1–6.

Figure	Particle	Centrality	T_0	β_T	N_0	χ^2	dof
Figure 1 Au-Au 7.7 GeV	π^+	0–5%	0.130 ± 0.004	0.306 ± 0.006	15.00 ± 1.00	17	26
		5–10%	0.129 ± 0.005	0.305 ± 0.005	6.02 ± 0.9	14	26
		10–20%	0.128 ± 0.004	0.303 ± 0.007	2.35 ± 1.05	20	26
		20–30%	0.126 ± 0.005	0.302 ± 0.006	1.09 ± 0.60	18	26
		30–40%	0.124 ± 0.004	0.300 ± 0.006	0.54 ± 0.43	19	23
		40–50%	0.122 ± 0.003	0.297 ± 0.007	0.28 ± 0.02	13	23
		50–60%	0.120 ± 0.004	0.292 ± 0.004	0.14 ± 0.02	20	22
		60–70%	0.118 ± 0.004	0.280 ± 0.005	0.067 ± 0.001	16	21
		70–80%	0.115 ± 0.005	0.269 ± 0.007	0.030 ± 0.008	11	18
	K^+	0–5%	0.133 ± 0.005	0.305 ± 0.005	3.65 ± 0.20	99	20
		5–10%	0.131 ± 0.004	0.304 ± 0.005	1.50 ± 0.15	76	22
		10–20%	0.130 ± 0.004	0.302 ± 0.007	0.53 ± 0.05	55	22
		20–30%	0.128 ± 0.005	0.301 ± 0.007	0.24 ± 0.17	27	22
		30–40%	0.127 ± 0.004	0.299 ± 0.009	0.11 ± 0.01	27	21
		40–50%	0.125 ± 0.006	0.296 ± 0.008	0.050 ± 0.002	16	20
		50–60%	0.123 ± 0.005	0.278 ± 0.007	0.23 ± 0.02	34	19
		60–70%	0.118 ± 0.004	0.265 ± 0.008	0.0093 ± 0.0007	34	18
		70–80%	0.116 ± 0.004	0.250 ± 0.008	0.0034 ± 0.0003	29	15
	p	0–5%	0.134 ± 0.004	0.340 ± 0.005	9.31 ± 0.60	54	29
		5–10%	0.133 ± 0.005	0.328 ± 0.006	3.90 ± 0.15	47	29
		10–20%	0.132 ± 0.006	0.318 ± 0.008	1.50 ± 0.20	46	29
		20–30%	0.130 ± 0.005	0.310 ± 0.008	0.65 ± 0.05	28	29
		30–40%	0.128 ± 0.004	0.301 ± 0.006	0.32 ± 0.04	14	25
		40–50%	0.126 ± 0.005	0.280 ± 0.007	0.15 ± 0.03	13	25
		50–60%	0.124 ± 0.004	0.271 ± 0.006	0.070 ± 0.008	7	24
		60–70%	0.122 ± 0.003	0.250 ± 0.005	0.030 ± 0.004	8	25
		70–80%	0.120 ± 0.006	0.204 ± 0.009	0.013 ± 0.001	14	18
Figure 2 Au-Au 11.5 GeV	π^+	0–5%	0.132 ± 0.004	0.315 ± 0.005	19.11 ± 1.60	5	26
		5–10%	0.130 ± 0.005	0.313 ± 0.005	7.60 ± 1.40	16	26
		10–20%	0.129 ± 0.004	0.312 ± 0.006	2.90 ± 0.50	14	26
		20–30%	0.128 ± 0.003	0.311 ± 0.007	1.36 ± 0.10	34	26
		30–40%	0.127 ± 0.003	0.310 ± 0.008	0.38 ± 0.05	15	26
		40–50%	0.126 ± 0.006	0.307 ± 0.007	0.34 ± 0.03	16	26
		50–60%	0.124 ± 0.004	0.305 ± 0.005	0.16 ± 0.01	7	23
		60–70%	0.121 ± 0.004	0.296 ± 0.006	0.080 ± 0.007	6	21
		70–80%	0.119 ± 0.005	0.288 ± 0.008	0.040 ± 0.005	10	21
	K^+	0–5%	0.135 ± 0.005	0.314 ± 0.009	4.23 ± 0.30	64	22
		5–10%	0.133 ± 0.004	0.312 ± 0.008	1.72 ± 0.10	62	23
		10–20%	0.132 ± 0.006	0.310 ± 0.010	0.60 ± 0.05	46	23
		20–30%	0.130 ± 0.003	0.308 ± 0.004	0.27 ± 0.02	45	23
		30–40%	0.129 ± 0.004	0.307 ± 0.006	0.13 ± 0.01	59	23
		40–50%	0.128 ± 0.005	0.306 ± 0.007	0.060 ± 0.006	11	23
		50–60%	0.126 ± 0.004	0.300 ± 0.006	0.026 ± 0.002	15	22

Table 1: Continued.

Figure	Particle	Centrality	T_0	β_T	N_0	χ^2	dof
		60–70%	0.124 ± 0.003	0.288 ± 0.005	0.011 ± 0.001	6	20
		70–80%	0.122 ± 0.004	0.264 ± 0.011	0.0050 ± 0.0003	26	19
	p	0–5%	0.136 ± 0.005	0.323 ± 0.007	7.74 ± 1.00	55	25
		5–10%	0.135 ± 0.005	0.321 ± 0.007	2.90 ± 0.25	56	26
		10–20%	0.134 ± 0.005	0.318 ± 0.006	1.12 ± 0.15	40	26
		20–30%	0.132 ± 0.004	0.311 ± 0.007	0.50 ± 0.03	24	26
		30–40%	0.130 ± 0.005	0.308 ± 0.007	0.24 ± 0.01	13	26
		40–50%	0.128 ± 0.003	0.285 ± 0.006	0.12 ± 0.01	10	25
		50–60%	0.125 ± 0.004	0.274 ± 0.008	0.55 ± 0.01	13	25
		60–70%	0.123 ± 0.00414	0.251 ± 0.006	0.024 ± 0.004	7	25
		70–80%	0.121 ± 0.004	0.231 ± 0.007	0.010 ± 0.003	23	26
	π^+	0–5%	0.135 ± 0.003	0.320 ± 0.005	22.14 ± 2.00	4	25
		5–10%	0.133 ± 0.003	0.318 ± 0.006	8.50 ± 2.00	10	25
		10–20%	0.132 ± 0.004	0.317 ± 0.006	3.50 ± 0.25	12	25
		20–30%	0.131 ± 0.004	0.315 ± 0.005	1.60 ± 0.13	15	25
		30–40%	0.130 ± 0.004	0.314 ± 0.007	0.80 ± 0.06	10	25
		40–50%	0.128 ± 0.004	0.311 ± 0.006	0.40 ± 0.03	16	25
		50–60%	0.126 ± 0.004	0.307 ± 0.007	0.19 ± 0.02	7	25
		60–70%	0.124 ± 0.004	0.299 ± 0.007	0.093 ± 0.014	8	25
		70–80%	0.120 ± 0.005	0.291 ± 0.005	0.040 ± 0.006	14	25
	K^+	0–5%	0.137 ± 0.005	0.318 ± 0.007	4.36 ± 0.40	16	23
		5–10%	0.136 ± 0.004	0.314 ± 0.008	1.86 ± 0.20	8	23
		10–20%	0.135 ± 0.005	0.313 ± 0.008	0.70 ± 0.08	21	23
Figure 3		20–30%	0.134 ± 0.004	0.312 ± 0.006	0.31 ± 0.03	15	23
Au-Au		30–40%	0.132 ± 0.004	0.310 ± 0.009	0.14 ± 0.01	9	23
14.5 GeV		40–50%	0.130 ± 0.003	0.308 ± 0.008	0.067 ± 0.006	7	21
		50–60%	0.128 ± 0.006	0.305 ± 0.010	0.025 ± 0.003	9	21
		60–70%	0.127 ± 0.004	0.294 ± 0.007	0.012 ± 0.001	3	19
		70–80%	0.125 ± 0.005	0.267 ± 0.008	0.0060 ± 0.0006	4	17
	p	0–5%	0.139 ± 0.005	0.335 ± 0.009	6.47 ± 0.70	22	23
		5–10%	0.137 ± 0.004	0.328 ± 0.008	2.90 ± 0.30	20	23
		10–20%	0.135 ± 0.003	0.326 ± 0.008	1.03 ± 0.12	18	23
		20–30%	0.134 ± 0.004	0.323 ± 0.007	0.46 ± 0.07	15	23
		30–40%	0.132 ± 0.004	0.315 ± 0.008	0.21 ± 0.03	12	23
		40–50%	0.130 ± 0.005	0.311 ± 0.007	0.096 ± 0.012	11	23
		50–60%	0.128 ± 0.005	0.294 ± 0.005	0.042 ± 0.007	13	23
		60–70%	0.126 ± 0.005	0.270 ± 0.008	0.018 ± 0.004	18	23
		70–80%	0.123 ± 0.004	0.236 ± 0.007	0.0080 ± 0.0019	26	23
	π^+	0–5%	0.138 ± 0.004	0.322 ± 0.004	24.14 ± 2.00	9	23
Figure 4		5–10%	0.137 ± 0.004	0.321 ± 0.005	9.50 ± 0.80	6	23
Au-Au		10–20%	0.135 ± 0.005	0.319 ± 0.008	3.75 ± 0.25	7	23
19.6 GeV		20–30%	0.134 ± 0.004	0.317 ± 0.005	1.97 ± 0.16	12	23
		30–40%	0.132 ± 0.003	0.315 ± 0.005	0.87 ± 0.06	18	23

Table 1: Continued.

Figure	Particle	Centrality	T_0	β_T	N_0	χ^2	dof
		40–50%	0.130 ± 0.004	0.312 ± 0.006	0.43 ± 0.04	20	23
		50–60%	0.129 ± 0.005	0.311 ± 0.008	0.22 ± 0.02	16	23
		60–70%	0.128 ± 0.004	0.308 ± 0.008	0.10 ± 0.01	16	23
		70–80%	0.125 ± 0.005	0.303 ± 0.009	0.048 ± 0.004	14	23
	K^+	0–5%	0.140 ± 0.003	0.320 ± 0.007	4.98 ± 0.30	24	23
		5–10%	0.138 ± 0.005	0.319 ± 0.009	2.00 ± 0.20	33	23
		10–20%	0.136 ± 0.005	0.318 ± 0.007	0.75 ± 0.05	33	23
		20–30%	0.135 ± 0.005	0.314 ± 0.007	0.34 ± 0.02	21	23
		30–40%	0.133 ± 0.004	0.311 ± 0.007	0.16 ± 0.03	12	23
		40–50%	0.130 ± 0.005	0.309 ± 0.009	0.075 ± 0.005	15	22
		50–60%	0.129 ± 0.004	0.307 ± 0.008	0.036 ± 0.005	8	22
		60–70%	0.128 ± 0.006	0.300 ± 0.010	0.016 ± 0.001	23	20
		70–80%	0.126 ± 0.004	0.294 ± 0.009	0.0070 ± 0.0003	25	19
	p	0–5%	0.142 ± 0.005	0.338 ± 0.006	5.84 ± 0.70	41	26
		5–10%	0.140 ± 0.006	0.336 ± 0.008	2.40 ± 0.30	28	22
		10–20%	0.138 ± 0.005	0.334 ± 0.005	0.91 ± 0.12	19	20
		20–30%	0.136 ± 0.005	0.324 ± 0.007	0.37 ± 0.06	41	20
		30–40%	0.133 ± 0.004	0.316 ± 0.005	0.18 ± 0.03	20	20
		40–50%	0.131 ± 0.006	0.312 ± 0.008	0.090 ± 0.016	8	20
		50–60%	0.129 ± 0.005	0.295 ± 0.009	0.042 ± 0.007	14	20
		60–70%	0.128 ± 0.004	0.275 ± 0.008	0.019 ± 0.003	2	20
		70–80%	0.125 ± 0.004	0.237 ± 0.007	0.0080 ± 0.0013	11	20
Figure 5 Au-Au 27 GeV	π^+	0–5%	0.139 ± 0.004	0.326 ± 0.006	26.14 ± 1.80	5	23
		5–10%	0.138 ± 0.004	0.324 ± 0.008	11.07 ± 2.00	8	23
		10–20%	0.136 ± 0.005	0.323 ± 0.004	4.25 ± 0.25	10	23
		20–30%	0.135 ± 0.004	0.322 ± 0.004	1.90 ± 0.15	14	23
		30–40%	0.133 ± 0.003	0.321 ± 0.004	0.98 ± 0.10	23	23
		40–50%	0.131 ± 0.004	0.320 ± 0.006	0.50 ± 0.03	26	23
		50–60%	0.130 ± 0.005	0.318 ± 0.005	0.23 ± 0.03	19	23
		60–70%	0.129 ± 0.005	0.317 ± 0.009	0.11 ± 0.01	21	23
		70–80%	0.128 ± 0.004	0.315 ± 0.005	0.048 ± 0.005	19	23
	K^+	0–5%	0.142 ± 0.005	0.324 ± 0.008	5.11 ± 0.60	53	23
		5–10%	0.140 ± 0.005	0.322 ± 0.007	2.15 ± 0.20	52	23
		10–20%	0.139 ± 0.003	0.321 ± 0.008	0.82 ± 0.10	55	23
		20–30%	0.137 ± 0.006	0.321 ± 0.005	0.37 ± 0.03	43	23
		30–40%	0.136 ± 0.004	0.320 ± 0.007	0.18 ± 0.01	25	23
		40–50%	0.134 ± 0.004	0.318 ± 0.008	0.86 ± 0.01	9	23
		50–60%	0.132 ± 0.005	0.316 ± 0.005	0.040 ± 0.005	8	23
		60–70%	0.130 ± 0.004	0.311 ± 0.006	0.014 ± 0.003	12	23
		70–80%	0.128 ± 0.004	0.304 ± 0.007	0.0070 ± 0.0004	27	23
	p	0–5%	0.144 ± 0.004	0.343 ± 0.007	5.31 ± 0.40	34	20
		5–10%	0.143 ± 0.004	0.341 ± 0.007	2.20 ± 0.22	27	20
		10–20%	0.141 ± 0.005	0.336 ± 0.007	0.84 ± 0.09	21	20

Table 1: Continued.

Figure	Particle	Centrality	T_0	β_T	N_0	χ^2	dof
		20–30%	0.139 ± 0.005	0.330 ± 0.006	0.37 ± 0.05	15	20
		30–40%	0.137 ± 0.005	0.326 ± 0.008	0.18 ± 0.03	9	20
		40–50%	0.134 ± 0.005	0.318 ± 0.005	0.090 ± 0.016	8	20
		50–60%	0.131 ± 0.004	0.300 ± 0.008	0.042 ± 0.005	3	20
		60–70%	0.129 ± 0.004	0.280 ± 0.005	0.019 ± 0.002	6	20
		70–80%	0.126 ± 0.004	0.257 ± 0.007	0.0070 ± 0.0003	9	20
	π^+	0–5%	0.141 ± 0.004	0.330 ± 0.007	27.84 ± 2.30	7	23
		5–10%	0.139 ± 0.005	0.328 ± 0.007	11.60 ± 0.70	14	23
		10–20%	0.138 ± 0.004	0.326 ± 0.006	4.50 ± 0.30	23	23
		20–30%	0.136 ± 0.004	0.325 ± 0.005	2.12 ± 0.10	38	23
		30–40%	0.135 ± 0.003	0.324 ± 0.008	1.05 ± 0.08	42	23
		40–50%	0.135 ± 0.005	0.322 ± 0.005	0.52 ± 0.02	36	23
		50–60%	0.134 ± 0.004	0.321 ± 0.008	0.27 ± 0.02	39	23
		60–70%	0.132 ± 0.004	0.320 ± 0.007	0.12 ± 0.01	36	23
		70–80%	0.130 ± 0.005	0.319 ± 0.008	0.062 ± 0.005	51	23
	K^+	0–5%	0.148 ± 0.004	0.328 ± 0.005	5.29 ± 0.40	35	23
		5–10%	0.147 ± 0.004	0.327 ± 0.006	2.30 ± 0.15	15	23
		10–20%	0.146 ± 0.005	0.328 ± 0.005	0.90 ± 0.08	29	23
Figure 6		20–30%	0.145 ± 0.006	0.324 ± 0.009	0.40 ± 0.03	19	23
Au-Au		30–40%	0.144 ± 0.005	0.323 ± 0.008	0.19 ± 0.01	12	23
39 GeV		40–50%	0.143 ± 0.005	0.321 ± 0.006	0.090 ± 0.010	10	23
		50–60%	0.142 ± 0.003	0.317 ± 0.006	0.0040 ± 0.0004	12	23
		60–70%	0.140 ± 0.004	0.316 ± 0.005	0.019 ± 0.001	15	23
		70–80%	0.138 ± 0.005	0.313 ± 0.008	0.0083 ± 0.0003	18	23
	p	0–5%	0.149 ± 0.005	0.359 ± 0.008	4.38 ± 0.50	34	19
		5–10%	0.148 ± 0.004	0.348 ± 0.006	1.94 ± 0.30	36	19
		10–20%	0.146 ± 0.005	0.346 ± 0.006	0.80 ± 0.12	22	19
		20–30%	0.145 ± 0.004	0.340 ± 0.007	0.33 ± 0.05	16	19
		30–40%	0.144 ± 0.004	0.335 ± 0.005	0.16 ± 0.03	8	19
		40–50%	0.144 ± 0.004	0.330 ± 0.006	0.078 ± 0.014	13	19
		50–60%	0.143 ± 0.004	0.300 ± 0.006	0.040 ± 0.005	1	19
		60–70%	0.139 ± 0.004	0.281 ± 0.005	0.017 ± 0.002	4	19
		70–80%	0.127 ± 0.004	0.274 ± 0.007	0.0080 ± 0.0006	10	19

It is hard to say whether the minimum or maximum point of EoS of the matter formed in the most central Au-Au collisions at 11.5 GeV is related to the search for the QCD critical end point (CEP) which is the main objective of the BES program performed by the STAR Collaboration. Generally, large nonmonotonous changes or saturations or a slight increase should appear in the excitation functions of some quantities at the critical energy which is the energy corresponding to the CEP. The excitation functions considered in this paper change slightly. Although there is no value in the energy range of less than 7.7 GeV, it is expected that the excitation function increases quickly in the energy range of a few GeV while the onset stage of a slight increase appears at around 10 GeV in the excitation functions of $\langle p_T \rangle$ and T_i.

It should be noted that there is entanglement in the extraction of T_0 and β_T. In fact, if one uses smaller T_0 and larger β_T for central collisions, a decreasing trend for T_0 from peripheral to central collisions can be obtained. Meanwhile, a negative correlation between T_0 and β_T can also be obtained. Thus, this situation is in agreement with some current references [19, 55, 56]. If one even uses almost invariant or slightly larger T_0 and properly larger β_T for central collisions, an almost invariant or slightly increased trend for T_0 from peripheral to central collisions can be obtained [57]. To show

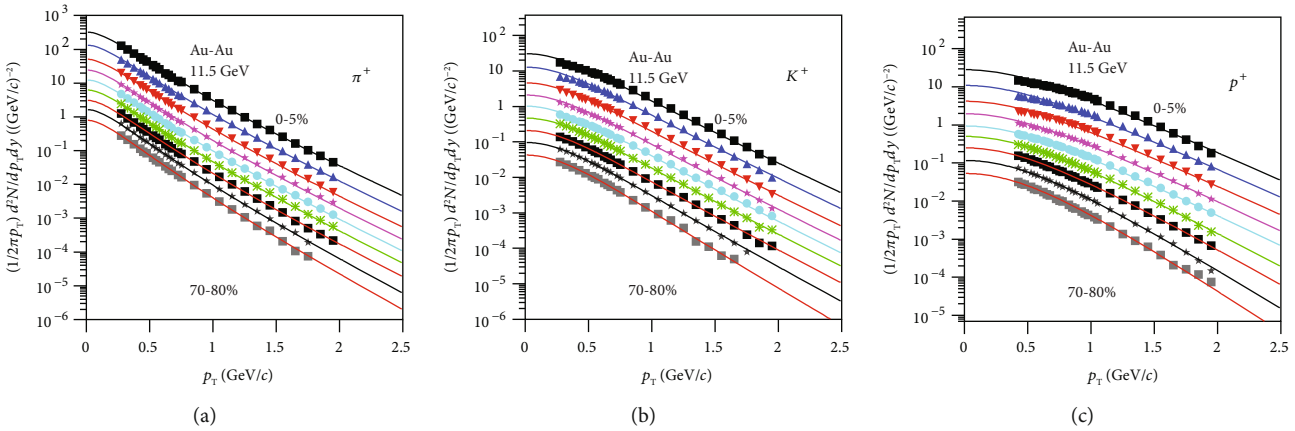

FIGURE 2: The same as Figure 1, but showing the results at $\sqrt{sNN} = 11.5$ GeV.

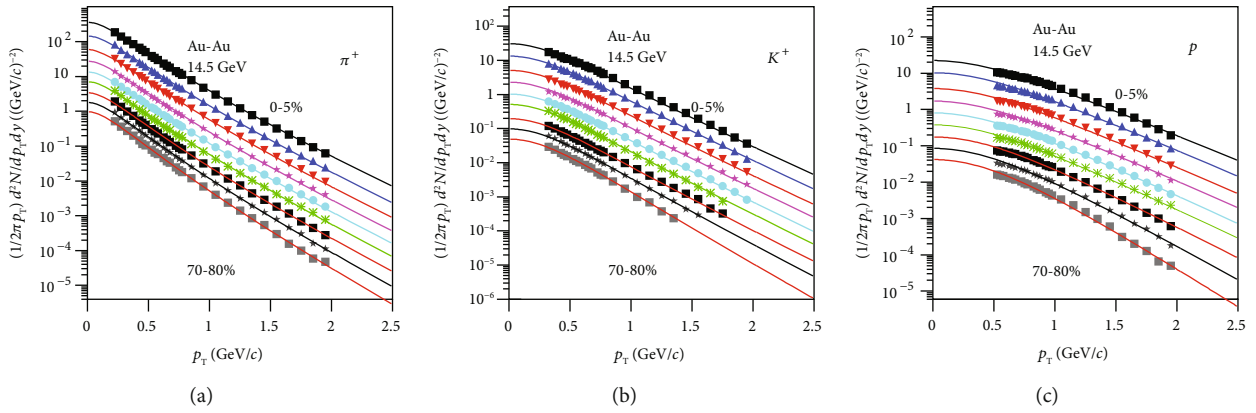

FIGURE 3: The same as Figure 1, but showing the results at $\sqrt{sNN} = 14.5$ GeV, where the data are cited from Ref. [20].

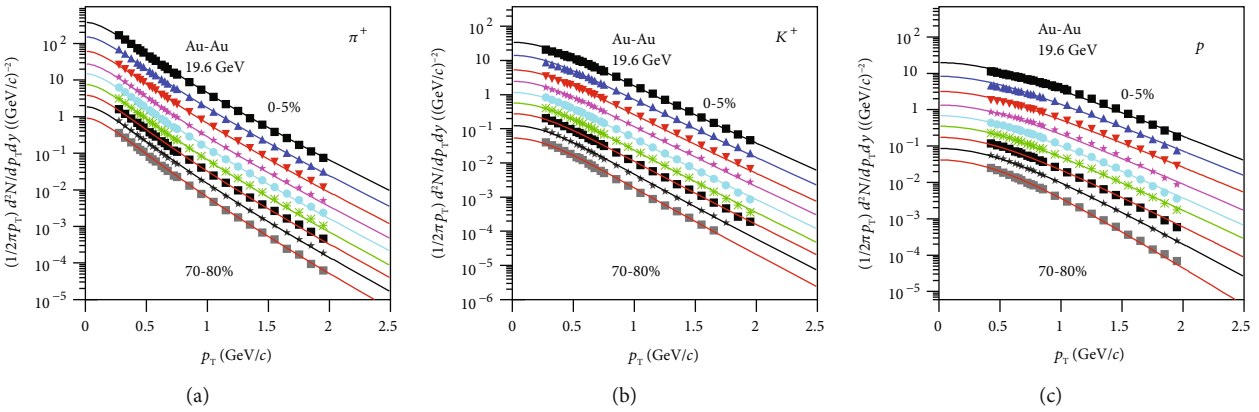

FIGURE 4: The same as Figure 1, but showing the results at $\sqrt{sNN} = 19.6$ GeV.

the flexibility in the extraction of T_0 and β_T, this work has reported an increasing trend for T_0 from peripheral to central collisions and a positive correlation between T_0 and β_T.

In addition, we have taken $n_0 = 2$ in this work, which closely resembles the hydrodynamic profile as mentioned in Ref. [21]. Although Ref. [58] shows that $n_0 = 1$ is the closest approximation to hydrodynamics at freeze-out, Ref. [36] shows that $n_0 = 2$ or 1 does not affect obviously the fit curve and free parameters T_0 and β_T. If we consider that $\beta(r)$ decays quickly from the surface to the center of the emission source, we are inclined to use $n_0 = 2$. Anyhow, we are not inclined to regard n_0 as a free parameter which is too mutable and debatable in our opinion. In current analysis with the blast-wave model [22], not only is n_0 mutable (from $0.0 \pm$

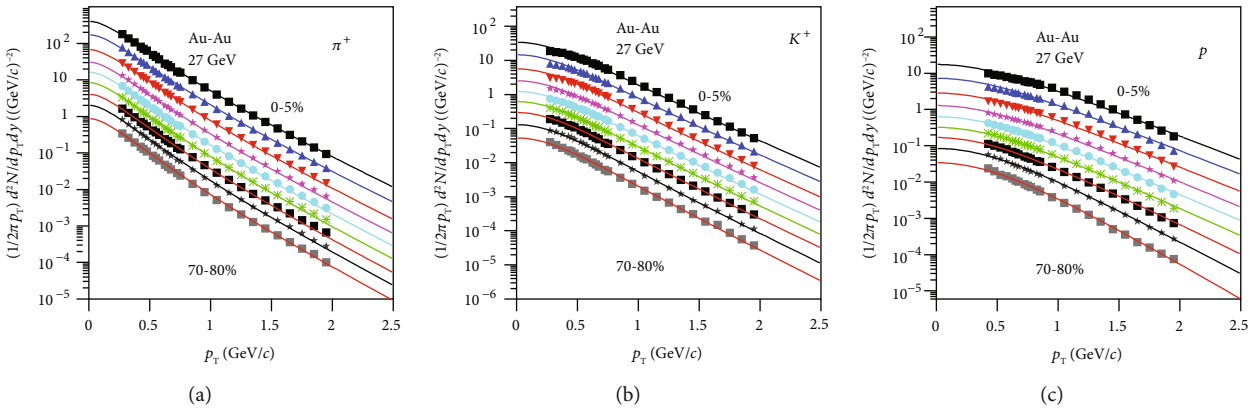

Figure 5: The same as Figure 1, but showing the results at $\sqrt{sNN} = 27$ GeV.

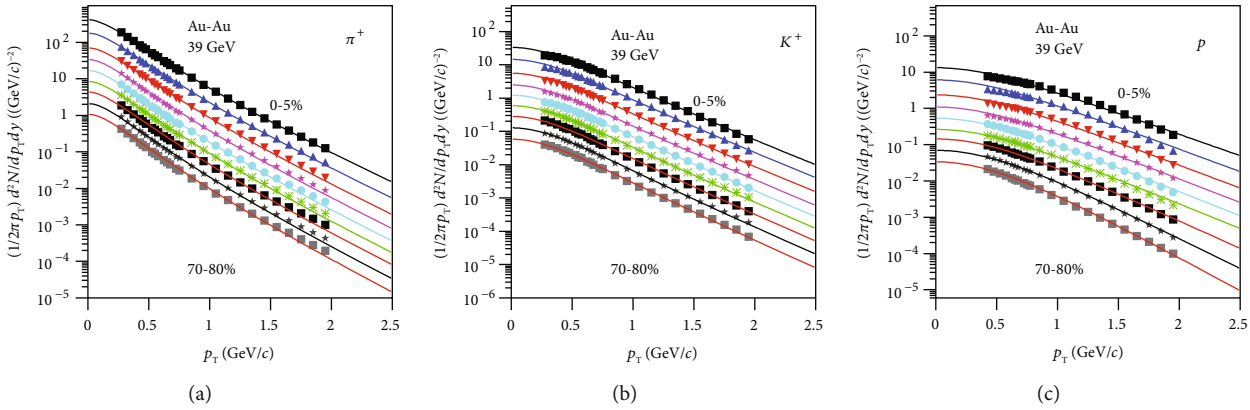

Figure 6: The same as Figure 1, but showing the results at $\sqrt{sNN} = 39$ GeV.

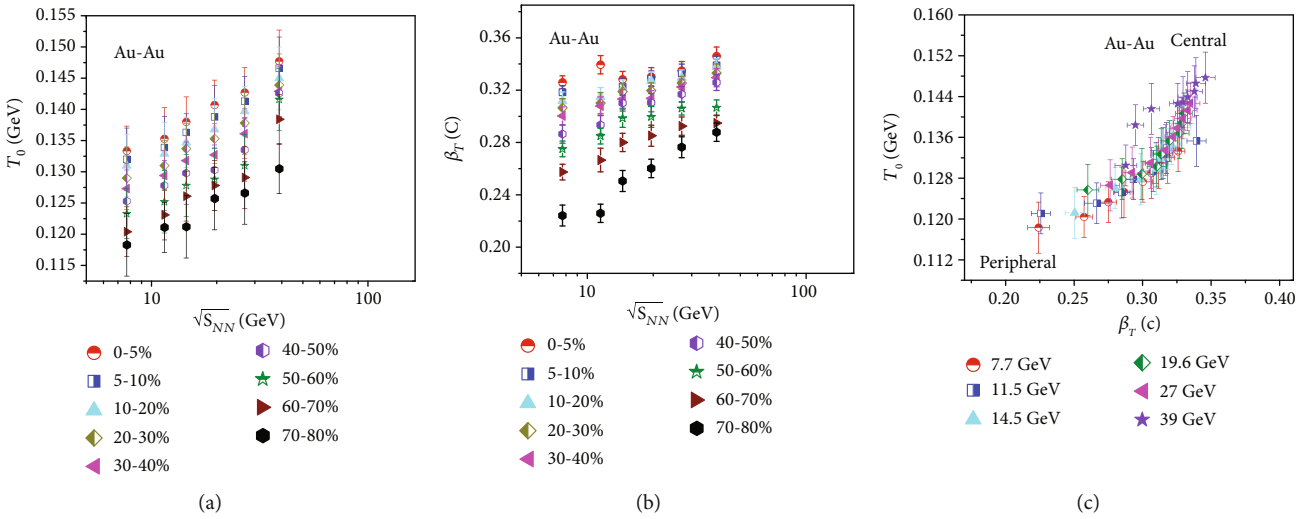

Figure 7: Dependences of weighted averages (a) T_0 and (b) β_T on $\sqrt{sNN}$ for different event centralities as well as (c) T_0 on β_T for different collision energies and event centralities. The different symbols display different centrality classes in (a) and (b) or different collision energies in (c), which are averaged by weighting the yields of different particles which are listed in Table 1.

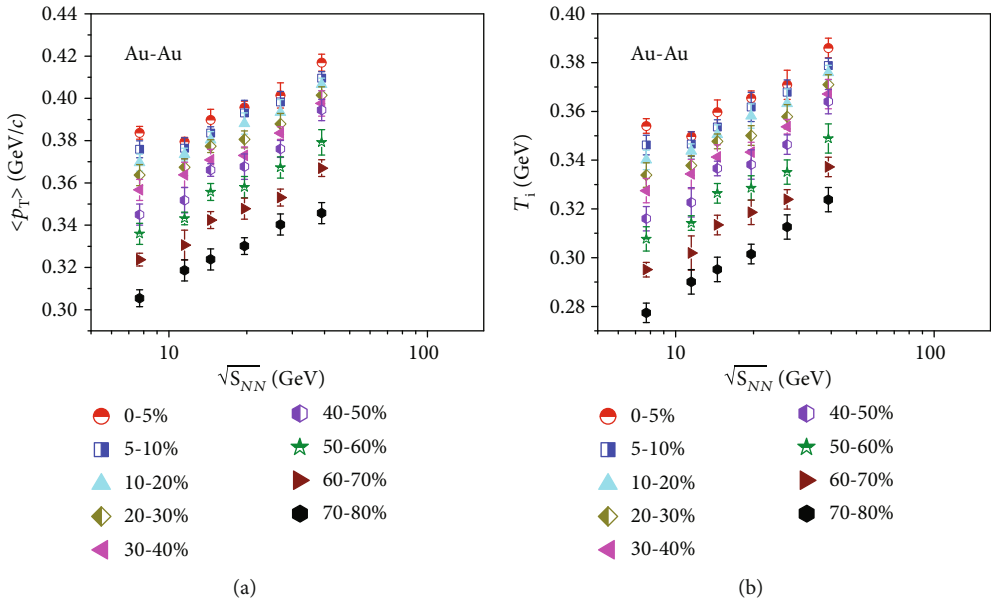

FIGURE 8: Dependences of weighted averages (a) $\langle p_T \rangle$ and (b) T_i on $\sqrt{sNN}$ for different event centralities. The different symbols display different centrality classes, which are averaged by weighting the yields of different particles which are listed in Table 1.

10.1 to 4.3 ± 1.7) but also the p_T coverage is narrow and particle-dependent ($p_T \approx 0.20 - 0.70$ GeV/c for π^+, 0.25 – 0.75 GeV/c for K^+, and 0.35 – 1.15 GeV/c for p), which uses a single kinetic freeze-out scenario and results in different trends of T_0 versus β_T from this work. If we also regard n_0 as a free parameter and use narrow and particle-dependent p_T coverage, consistent result with current analysis [22] can be naturally obtained by us.

Indeed, there are too much uncertainties arising from the choice of fit function and flow profile and from the well-known ambiguity in the fit results—in a single p_T spectrum, it is always possible to trade β_T against T_0. That is, T_0 and β_T is negatively correlative for a given p_T spectrum. It is possible that we may use suitable T_0 and β_T for a set of p_T spectra and obtain a positive or negative correlation. In a positive correlation, decreasing T_0 and increasing β_T will result in a negative correlation. Contrarily, in a negative correlation, increasing T_0 and decreasing β_T will result in a positive correlation. Indeed, there is an influence if we use a changeable p_T coverage and/or n_0 choice on the extraction of the two free parameters. In our opinion, to reduce the uncertainties, one should use a fixed flow profile (n_0) and wide and fixed p_T coverage for different particles. In fact, we have used $n_0 = 2$ and $p_T < 2.5$ GeV/c for different particles in this work and used a multiple freeze-out scenario such as that used in Ref. [59].

Our result (Table 1) shows that the heavier the particle is, the higher T_0 and the smaller β_T correspond. This result is in agreement with the hydrodynamic-type behavior [4]. The final T_0 and β_T are averaged by weighting different particle yields, which shows a positive correlation between T_0 and β_T (Figure 7). Our result is in agreement with the alternative method [36, 37] in which T_0 is regarded as the intercept in the linear relation of T versus m_0 and β_T is regarded as the slope in the linear relation of $\langle p_T \rangle$ versus $m_0\bar{\gamma}$, where $\bar{\gamma}$ is the mean Lorentz factor in the source rest frame. Our result is also in agreement with a very recent work [60] which uses the same method as ours. If the negative correlation can be explained as the result of a longer lifetime (lower excitation degree) which corresponds to lower T_0 and a quicker expansion (stronger squeeze) which corresponds to larger β_T, the positive correlation can be explained as the result of a high excitation degree which corresponds to high T_0 and quick expansion (strong squeeze) which corresponds to large β_T.

This whole phenomenal analysis results in degrees of thermal motion and collective expansion that are reflected by T_0 and β_T, respectively. With the increasing collision energy, the system may undergo different evolution processes. In the considered RHIC-BES energy range, the violent degree of collisions increases with increasing collision energy. The trends of T_0 and β_T show approximately monotonous increase in which large fluctuation does not appear, though there are nonmonotonous changes at 11.5 GeV in some cases. The evolution processes at the considered six energies show similar behaviors to each other.

4. Conclusions

The main observations and conclusions are summarized as follows.

(a) By using the method of data-driven reanalysis, the blast-wave model with the Boltzmann-Gibbs statistics is used to analyze the collision energy-dependent and event centrality-dependent double-differential transverse momentum spectra of charged particles (π^+, K^+, and p) produced in the midrapidity interval in Au-Au collisions at the RHIC-BES energies. The contribution of soft excitation is considered in this

work, but the contribution of the hard process is not excluded if available

(b) As the free parameters, the kinetic freeze-out temperature T_0 and transverse flow velocity β_T are extracted with the blast-wave model. Both T_0 and β_T increase with the increase in collision energy due to more violent collisions at higher energy. The two parameters also increase with the increase in event centrality, as the central collisions contain more nucleons which means more energy deposited and more violent collisions and squeeze, compared with peripheral collisions

(c) As the derived parameters, the mean transverse momentum $\langle p_T \rangle$ and initial temperature T_i appear to be similar law to the free parameters T_0 and β_T when we study the dependences of parameters on collision energy and event centrality. Although T_0 and β_T are model-dependent, $\langle p_T \rangle$ and T_i are generally model-independent. There is no large fluctuation in the excitation function of the considered parameters at the RHIC-BES, which means a similar collision mechanism

Data Availability

The data used to support the findings of this study are included within the article and are cited at relevant places within the text as references.

Ethical Approval

The authors declare that they are in compliance with ethical standards regarding the content of this paper.

Disclosure

The funding agencies have no role in the design of the study; in the collection, analysis, or interpretation of the data; in the writing of the manuscript; or in the decision to publish the results.

Conflicts of Interest

The authors declare that there are no conflicts of interest regarding the publication of this paper.

Acknowledgments

We thank Dr. Muhammad Usman Ashraf for his kind help. This work was supported by the National Natural Science Foundation of China under Grant No. 11575103, the Chinese Government Scholarship (China Scholarship Council), the Scientific and Technological Innovation Programs (STIP) of Higher Education Institutions in Shanxi under Grant No. 201802017, the Shanxi Provincial Natural Science Foundation under Grant No. 201701D121005, and the Fund for Shanxi "1331 Project" Key Subjects Construction.

References

[1] S. Mukherjee and V. Skokov, "Universality driven analytic structure of QCD crossover: radius of convergence in baryon chemical potential," https://arxiv.org/abs/1909.04639.

[2] W.-J. Fu, J. M. Pawlowski, and F. Rennecke, "The QCD phase structure at finite temperature and density," https://arxiv.org/abs/1909.02991.

[3] G.-Y. Shao, W.-B. He, and X.-Y. Gao, "Deformed QCD phase structure and entropy oscillation in the presence of a magnetic background," *Physical Review D*, vol. 100, no. 1, article 014020, 2019.

[4] R. Sahoo, "Possible formation of QGP-droplets in proton-proton collisions at the CERN Large Hadron Collider," *AAPPS Bulletin*, vol. 29, no. 4, 2019.

[5] M. Gyulassy and L. McLerran, "New forms of QCD matter discovered at RHIC," *Nuclear Physics A*, vol. 750, no. 1, pp. 30–63, 2005.

[6] M. T. AlFiky, O. T. ElSherif, and A. M. Hamed, "Quark gluon plasma formation in proton-proton collisions using PYTHIA," https://arxiv.org/abs/1902.05114.

[7] F. Rennecke, W.-J. Fu, and J. M. Pawlowski, "Strangeness neutrality and the QCD phase diagram," https://arxiv.org/abs/1907.08179.

[8] A. Andronic, P. Braun-Munzinger, and J. Stachel, "Hadron production in central nucleus–nucleus collisions at chemical freeze-out," *Nuclear Physics A*, vol. 772, no. 3-4, pp. 167–199, 2006.

[9] G. Inghirami, P. Hillmann, B. Tomášik, and M. Bleicher, "Temperatures and chemical potentials at kinetic freeze-out in relativistic heavy ion collisions from coarse grained transport simulations," https://arxiv.org/abs/1909.00643.

[10] C. Yang, "The STAR detector upgrades and physics in beam energy scan phase II," *EPJ Web of Conferences*, vol. 182, article 02130, p. 02130, 2018.

[11] K. C. Meehan, "Fixed target collisions at STAR," *Nuclear Physics A*, vol. 956, pp. 878–881, 2016.

[12] X. Sun and the STAR Collaboration, "Flow in the RHIC Beam Energy Scan from STAR," *Journal of Physics: Conference Series*, vol. 535, article 012005, 2014.

[13] K. C. Meehan, "The fixed-target experiment at STAR," *Journal of Physics: Conference Series*, vol. 742, article 012022, 2016.

[14] T. Ablyazimov, A. Abuhoza, R. P. Adak et al., "Challenges in QCD matter physics – the scientific programme of the Compressed Baryonic Matter experiment at FAIR," *The European Physical Journal A*, vol. 53, p. 60, 2017.

[15] J. Chen, D. Keane, Y. G. Ma, A. Tang, and Z. Xu, "Antinuclei in heavy-ion collisions," *Physics Reports*, vol. 760, pp. 1–39, 2018.

[16] N. Xu, "An overview of STAR experimental results," *Nuclear Physics A*, vol. 931, pp. 1–12, 2014.

[17] S. Chatterjee, S. Das, L. Kumar et al., "Freeze-out parameters in heavy-ion collisions at AGS, SPS, RHIC, and LHC energies," *Advances in High Energy Physics*, vol. 2015, Article ID 349013, 20 pages, 2015.

[18] S. Uddin, I. Bashir, and R. A. Bhat, "Transverse momentum distributions of hadrons produced in Pb-Pb collisions at LHC energy $\sqrt{s_{NN}} = 2.76$ TeV," *Advances in High Energy Physics*, vol. 2015, Article ID 154853, 7 pages, 2015.

[19] L. Adamczyk, J. K. Adkins, G. Agakishiev et al., "Bulk properties of the medium produced in relativistic heavy-ion collisions

from the Beam Energy Scan program," *Physical Review C*, vol. 96, no. 4, article 044904, 2017.

[20] V. Bairathi, "Study of the bulk properties of the system formed in Au + Au collisions at $\sqrt{s_{NN}} = 14.5$ GeV using the STAR detector at RHIC," *Nuclear Physics A*, vol. 956, pp. 292–295, 2016.

[21] E. Schnedermann, J. Sollfrank, and U. Heinz, "Thermal phenomenology of hadrons from 200*A* GeV S+S collisions," *Physical Review C*, vol. 48, no. 5, pp. 2462–2475, 1993.

[22] B. I. Abelev, M. M. Aggarwal, Z. Ahammed et al., "Systematic measurements of identified particle spectra in *pp*, *d* + Au, and Au+Au collisions at the STAR detector," *Physical Review C*, vol. 79, no. 3, article 034909, 2009.

[23] B. I. Abelev, M. M. Aggarwal, Z. Ahammed et al., "Identified particle production, azimuthal anisotropy, and interferometry measurements in Au + Au collisions at $\sqrt{s_{NN}} = 9.2$ GeV," *Physical Review C*, vol. 81, no. 2, article 024911, 2010.

[24] Z. Tang, Y. Xu, L. Ruan, G. van Buren, F. Wang, and Z. Xu, "Spectra and radial flow in relativistic heavy ion collisions with Tsallis statistics in a blast-wave description," *Physical Review C*, vol. 79, no. 5, article 051901, 2009.

[25] Z.-B. Tang, L. Yi, L. J. Ruan et al., "The statistical origin of constituent-quark scaling in QGP hadronization," *Chinese Physics Letters*, vol. 30, no. 3, article 031201, 2013.

[26] K. Jiang, Y. Zhu, W. Liu et al., "Onset of radial flow in $p + p$ collisions," *Physical Review C*, vol. 91, no. 2, article 024910, 2015.

[27] S. Takeuchi, K. Murase, T. Hirano, P. Huovinen, and Y. Nara, "Effects of hadronic rescattering on multistrange hadrons in high-energy nuclear collisions," *Physical Review C*, vol. 92, no. 4, article 044907, 2015.

[28] H. Heiselberg and A.-M. Levy, "Elliptic flow and Hanbury-Brown–Twiss correlations in noncentral nuclear collisions," *Physical Review C*, vol. 59, no. 5, pp. 2716–2727, 1999.

[29] U. W. Heinz, "Hydrodynamics at RHIC: how well does it work, where and how does it break down?," *Journal of Physics G: Nuclear and Particle Physics*, vol. 31, no. 6, article S717, 2005.

[30] R. Russo, "Measurement of D+ meson production in pPb collisions with the ALICE detector," 2015, https://arxiv.org/abs/1511.04380.

[31] S. Sadhu and P. Ghosh, "Anomalous features of particle production in high-multiplicity events of *pp* collisions at the LHC energies," *Physical Review D*, vol. 99, no. 3, article 034020, 2019.

[32] G. Bíró, G. Barnaföldi, T. Biró, K. Ürmössy, and Á. Takács, "Systematic analysis of the non-extensive statistical approach in high energy particle collisions - experiment vs. theory," *Entropy*, vol. 19, no. 3, article e19030088, p. 88, 2017.

[33] H.-R. Wei, F.-H. Liu, and R. A. Lacey, "Disentangling random thermal motion of particles and collective expansion of source from transverse momentum spectra in high energy collisions," *Journal of Physics G: Nuclear and Particle Physics*, vol. 43, no. 12, article 125102, 2016.

[34] H.-R. Wei, F.-H. Liu, and R. A. Lacey, "Kinetic freeze-out temperature and flow velocity extracted from transverse momentum spectra of final-state light flavor particles produced in collisions at RHIC and LHC," *The European Physical Journal A*, vol. 52, no. 4, p. 102, 2016.

[35] H.-L. Lao, H.-R. Wei, F.-H. Liu, and R. A. Lacey, "An evidence of mass-dependent differential kinetic freeze-out scenario observed in Pb-Pb collisions at 2.76 TeV," *The European Physical Journal A*, vol. 52, no. 7, p. 203, 2016.

[36] H.-L. Lao, F.-H. Liu, B.-C. Li, and M.-Y. Duan, "Kinetic freeze-out temperatures in central and peripheral collisions: which one is larger?," *Nuclear Science and Techniques*, vol. 29, no. 6, p. 82, 2018.

[37] H.-L. Lao, F.-H. Liu, B.-C. Li, M.-Y. Duan, and R. A. Lacey, "Examining the model dependence of the determination of kinetic freeze-out temperature and transverse flow velocity in small collision system," *Nuclear Science and Techniques*, vol. 29, no. 11, p. 164, 2018.

[38] J. Cleymans and D. Worku, "Relativistic thermodynamics: transverse momentum distributions in high-energy physics," *The European Physical Journal A*, vol. 48, no. 11, p. 160, 2012.

[39] H. Zheng and L. Zhu, "Comparing the Tsallis distribution with and without thermodynamical description in $p + p$ collisions," *Advances in High Energy Physics*, vol. 2016, Article ID 9632126, 10 pages, 2016.

[40] R. Hagedorn, "Multiplicities, p_T distributions and the expected hadron → quark-gluon phase transition," *La Rivista del Nuovo Cimento*, vol. 6, no. 10, pp. 1–50, 1983.

[41] ALICE Collaboration, B. Abelev, J. Adam et al., "Production of $\sum(1385)^{\pm}$ and $\Xi(1530)^{0}$ in proton–proton collisions at $\sqrt{s} = 7$ TeV," *The European Physical Journal C*, vol. 75, no. 1, p. 1, 2015.

[42] R. L. Ray and A. Jentsch, "Phenomenological models of two-particle correlation distributions on transverse momentum in relativistic heavy-ion collisions," *Physical Review C*, vol. 99, no. 2, article 024911, 2019.

[43] The CMS Collaboration, S. Chatrchyan, V. Khachatryan et al., "Study of high-p_T charged particle suppression in PbPb compared to pp collisions at $\sqrt{s_{NN}} = 2.76$ TeV," *The European Physical Journal C*, vol. 72, no. 3, 2012.

[44] C. Tsallis, "Possible generalization of Boltzmann-Gibbs statistics," *Journal of Statistical Physics*, vol. 52, no. 1-2, pp. 479–487, 1988.

[45] B. I. Abelev, J. Adams, M. M. Aggarwal et al., "Strange particle production in $p + p$ collisions at $\sqrt{s} = 200$ GeV," *Physical Review C*, vol. 75, no. 6, article 064901, 2007.

[46] T. S. Biró, G. Purcsel, and K. Urmössy, "Non-extensive approach to quark matter," *The European Physical Journal A*, vol. 40, no. 3, p. 325, 2009.

[47] R. Odorico, "Does a transverse energy trigger actually trigger on large-P_T jets?," *Physics Letters B*, vol. 118, no. 1-3, pp. 151–154, 1982.

[48] G. Arnison, A. Astbury, B. Aubert et al., "Transverse momentum spectra for charged particles at the CERN proton-antiproton collider," *Physics Letters B*, vol. 118, no. 1-3, pp. 167–172, 1982.

[49] T. Mizoguchi, M. Biyajima, and N. Suzuki, "Analyses of whole transverse momentum distributions in $p\bar{p}$ and pp collisions by using a modified version of Hagedorn's formula," *International Journal of Modern Physics A*, vol. 32, no. 11, article 1750057, 2017.

[50] M. Suleymanov, "The meaning behind observed p_T regions at the LHC energies," *International Journal of Modern Physics E*, vol. 27, no. 1, article 1850008, 2018.

[51] L. J. Gutay, A. S. Hirsch, R. P. Scharenberg, B. K. Srivastava, and C. Pajares, "De-confinement in small systems: clustering of color sources in high multiplicity $\bar{p}p$ collisions at $\sqrt{s} = 1.8$

TeV," *International Journal of Modern Physics E*, vol. 24, no. 12, article 1550101, 2015.

[52] A. S. Hirsch, C. Pajares, R. P. Scharenberg, and B. K. Srivastava, "De-confinement in high multiplicity proton-proton collisions at LHC energies," 2018, https://arxiv.org/abs/1803.02301.

[53] P. Sahoo, S. De, S. K. Tiwari, and R. Sahoo, "Energy and centrality dependent study of deconfinement phase transition in a color string percolation approach at RHIC energies," *The European Physical Journal A*, vol. 54, no. 8, p. 136, 2018.

[54] J. Cleymans, "The physics case for the $\sqrt{s_{NN}} \approx 10$ GeV region," 2017, http://arxiv.org/abs/1711.02882.

[55] B. Abelev, J. Adam, D. Adamová et al., "Centrality dependence of π, K, and p production in Pb-Pb collisions at $\sqrt{s_{NN}} = 2.76$ TeV," *Physical Review C*, vol. 88, no. 4, article 044910, 2013.

[56] L. Kumar, "Systematics of kinetic freeze-out properties in high energy collisions from STAR," *Nuclear Physics A*, vol. 931, pp. 1114–1119, 2014.

[57] A. Khuntia, H. Sharma, S. K. Tiwari, R. Sahoo, and J. Cleymans, "Radial flow and differential freeze-out in proton-proton collisions at $\sqrt{s} = 7$ TeV at the LHC," *The European Physical Journal A*, vol. 55, p. 3, 2019.

[58] P. F. Kolb and U. Heinz, "Hydrodynamic description of ultrarelativistic heavy-ion collisions," in *Quark-Gluon Plasma 3*, R. C. Hwa and X.-N. Wang, Eds., p. 788, World Scientific, Singapore, 2004.

[59] D. Thakur, S. Tripathy, P. Garg, R. Sahoo, and J. Cleymans, "Indication of a differential freeze-out in proton-proton and heavy-ion collisions at RHIC and LHC energies," *Advances in High Energy Physics*, vol. 2016, Article ID 4149352, 13 pages, 2016.

[60] P.-P. Yang, M.-Y. Duan, F.-H. Liu, and R. Sahoo, "Multiparticle production and initial quasi-temperature from proton induced carbon collisions at $p_{Lab} = 31$ GeV/c," https://arxiv.org/abs/1903.04008.